Chemical Engineering Journal 110 (2005) 1–10

Chemical Engineering Journal

www.elsevier.com/locate/cej

Parametric study of microreactor design for water gas shift reactor using an integrated reaction and heat exchange model

Gap-Yong Kim, J. Rhett Mayor*, Jun Ni

Department of Mechanical Engineering, University of Michigan, 2350 Hayward St., Ann Arbor, MI 48109, USA

Received 4 December 2003; accepted 17 May 2004

Abstract

This paper discusses the development of an integrated reaction and heat exchange approach to microreactor design that enhances reaction yields by allowing the reactant stream to follow optimal reactant temperature profiles. The paper details the formulation of both one-dimensional (1-D) and two-dimensional (2-D) models for the integrated reaction and heat exchange reactor design, and applies these models to a parametric study of microreactor designs for the water gas shift (WGS) reaction. The parametric study investigated the sensitivities of design parameters for both the parallel flow and counter flow configurations of the integrated reaction and heat exchange design. Results from the study are presented and discussed, and the preferred operating ranges of the parameters are identified for both configurations. A key finding of this study is the identification of the marked extension of the range of permissible wall thermal conductivities for high conversion efficiencies (greater than 85%) that is achieved by the counter flow integrated reactor configuration, thereby enabling the fabrication of microreactor components in conventional engineering materials. In addition, the integrated microreactor approach achieved higher catalyst utilization noted by a marked reduction in catalyst amount (of the order of 50%) when compared to a conventional adiabatic microreactor operating at the same level of conversion efficiency.

Keywords: Microreactor design; Water gas shift reaction; Integrated reaction and heat exchange

1. Introduction

In the drive towards the realization of a true hydrogen economy, the development of onboard fuel processing technologies for the future fuel cell-powered vehicles, both commercial and private, has become an area of increasing research focus. Onboard reforming capabilities have several positive attributes, including the ability to easily integrate with existing fuel infrastructures, improved power densities and thereby enhanced operation range and the avoidance of hydrogen storage challenges that make it an attractive alternative to onboard hydrogen fuel cell vehicles.

The fuel processor produces the hydrogen-rich streams required by the fuel cell from primary fuels that are converted in a multi-step reforming process. Typical fuel processors are comprised of a vaporizer/combustor, a primary reformer, a water gas shift (WGS) reactor and a carbon monoxide (CO) clean-up reactor. Critical issues in developing onboard fuel processor technology are the final size of the complete reformer and the start-up time, both of which need to be minimized.

Conventional fuel processing technology is based on fixed bed reactors, which tend to be very large in size, and therefore heat and mass transfer rates dominate and limit the observed reaction rates [1]. However, microchannel-based reactors can be small, efficient, modular and lightweight. The microchannels reduce the distance between the heat source and the heat sink, allowing for fast heat and mass transfer at the heat exchange and catalyst surface, respectively, in order to maintain the reactor at an optimal condition. This study focuses on the development of microchannel reactor models for one component of the fuel processor, the WGS reactor.

Prior research efforts directed at improving the performance of the WGS reaction have focused on a broad range of issues including the development of better catalysts [2],

* Corresponding author. Tel.: +1 734 763 5295; fax: +1 734 936 0363.
E-mail address: rmayor@powerixtech.com (J.R. Mayor).

1385-8947/$ – see front matter © 2005 Elsevier B.V. All rights reserved.
doi:10.1016/j.cej.2004.05.015

Nomenclature

Symbols

A_C	cross-sectional area (m^2)
A_{ku}	interfacial area of solid and fluid (m^2)
ΔA	incremental area (m^2)
b	width of the channel (m)
C_i	concentration of species i (mol/m^3)
C_P	heat capacity (J/kg K)
dx	incremental x (m)
dw	incremental weight of the catalyst (kg)
D_e	effective mass diffusion coefficient (m^2/s)
D_h	hydraulic diameter (m)
D_i	total diffusivity coefficient of species i (m^2/s)
D^d	mass dispersion coefficient (m^2/s)
F	molar flow rate (mol/s)
F_T	total molar flow rate (mol/s)
h	height of the channel/2 (m)
h_c	surface-convective heat transfer coefficient (W/m^2 K)
HtEx	abbreviation for 'heat exchange'
ΔH_{Rx}	heat of reaction (J/mol)
k_{cat}	thermal conductivity of the catalyst (W/m K)
k_e	effective thermal conductivity of the reactant (W/m K)
k_f	thermal conductivity of the fluid (W/m K)
k_w	thermal conductivity of the wall (W/m K)
k_3	specific reaction rate (mol/g s kPa^x)
L	length of the reactor (m)
mw	molecular weight of the reactant
Nu	Nusselt number
P	pressure (kPa)
Pe	Peclet number
Pr	Prandtl number
q	heat flux (W/m^2)
q'''	heat flux per unit volume of the reactor (W/m^3)
$\overline{q}$	molar flux (mol/m^2)
Q	volumetric heat generation (W/m^3)
r	reaction rate ($mol/s\ m^3$)
r'	reaction rate per weight of catalyst (mol/s g)
R	universal gas constant (8.314J/mol K)
Re	Reynolds number
s_n	normal vector to the surface
t	wall thickness (m)
T	temperature (Kelvin)
u	velocity (m/s)
u_D	Darcean velocity (m/s)
U	overall heat transfer coefficient (W/m^2 K)
V_s	volume of the solid (m^3)
ΔV	incremental volume (m^3)
Δx	incremental x (m)
Bold symbols	vectors

Greek letters

ε	porosity of the reactant bed
μ	viscosity (N s/m^2)
ρ	density (kg/m^3)
ρ_b	bulk catalyst density (g/m^3)
∇	differential operator $= \frac{\partial}{\partial x} i + \frac{\partial}{\partial y} j + \frac{\partial}{\partial z} k$

Subscripts

f	fluid
i	reactant species i
x	geometrical direction in x
y	geometrical direction in y
0	condition at the inlet ($x = 0$)
1	section 1: heat exchange stream
2	section 2: wall
3	section 3: reactant stream

experimental/theoretical studies to obtain kinetics of the catalyst [3,4], and heat and mass transfer studies in adiabatic/isothermal reactors [5]. In 1999, Tonkovich et al. investigated microchannel reactors with small parallel flow paths (100–1000 μm in width, with aspect ratios (channel height to width) between 1:1 and 100:1, and lengths of 1–10 cm) using monolithic catalysts fabricated on nickel foam monolith supports [1]. In their work, fast intrinsic kinetics were observed for the WGS reaction. However, detailed study into the characterization of WGS microreactors has received limited attention.

This study proposes an integrated reaction and heat exchange model for the microreactor-based WGS process. Both one-dimensional (1-D) and two-dimensional (2-D) models have been developed, and the formulations of the models are presented in Sections 2 and 3, respectively. Section 4 describes the rate equations and simulation conditions used in the paper. The models have been utilized to investigate the influence of various parameters of microreactor design on the performance of the process in terms of CO conversion and the results are presented in Sections 5–7. Key results are summarized in Section 8 with concluding remarks.

1.1. Water gas shift reaction

The WGS reaction is typically a heterogeneous reaction of gas phase reactant and solid phase catalyst, which is usually in the form of pellets through which the reactant stream flows. The purpose of the WGS reaction is to reduce the CO content of the reactant stream in order to avoid poisoning the catalysts in the fuel cell stack. The reaction, which is slightly exothermic, converts CO to carbon dioxide (CO_2) and hydrogen (H_2) as shown in Eq. (1).

$$CO + H_2O \Leftrightarrow CO_2 + H_2, \quad \Delta H_R < 0 \tag{1}$$

At low temperatures, the reaction favors the forward shift reaction, while at high temperatures the reverse reaction dominates. Typically, the WGS reaction is carried out in two stages, a low temperature shift (LTS) and a high temperature shift (HTS), which utilize different catalysts. The HTS catalysts operate at the temperature range of 320–450 °C, whereas the LTS catalysts operate at 200–250 °C [6].

Fig. 1 represents the relationship among conversion, temperature and reaction rate for a typical reversible exothermic reaction. The solid curves represent lines of constant rate. The reaction rate is zero along the equilibrium line and increases with temperature, as the mixture gets farther away from the equilibrium line. Therefore, the reaction rate must go through a maximum at some temperature below the equilibrium temperature [7]. As the value of the reaction rate increases, the maximum fractional conversion achievable in the reaction decreases. The manipulation of this characteristic suggests a route for minimizing the reactor volume. One can start the reaction at a high temperature to take advantage of the fast reaction rate, and then, progressively lower the temperature to increase the fractional conversion yield as illustrated by the dotted line in Fig. 1. It is possible, therefore, to determine an optimal temperature profile for the reactant stream that will provide a desired conversion for a minimum reactor volume [8].

However, achieving and maintaining the optimum temperature profile of the reactant stream in conventional size reactors is difficult due to complicated cooling designs and heat and mass transfer limitations. Consequently, multistage reactor schemes are often employed for practical applications. A possible pathway of a multistage reactor is depicted in Fig. 1 as a solid line. The first adiabatic reactor can only reach low conversion, X_1. The reacting stream is then cooled in an interstage heat exchanger, and flowed through the second adiabatic reactor, where higher conversion, X_2, is achieved. It can be observed that even with multistage reactors the majority of the catalyst is either below or above the optimum temperature, which occupies unnecessary reactor volume. However, with microscale reactors, heat and mass transfer limitations may be overcome through the beneficial scaling effects of miniaturization; at the smaller length scales, the thermal response time is significantly reduced.

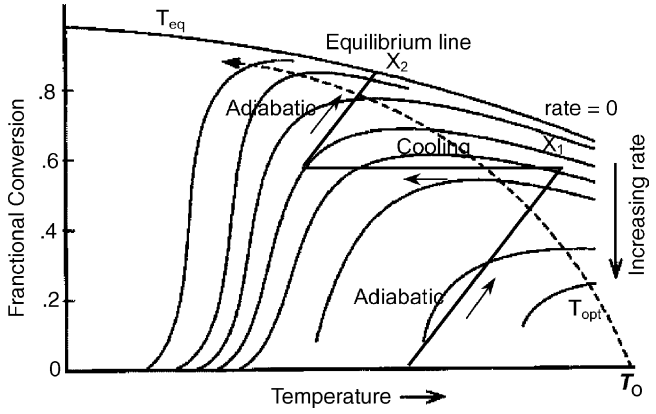

Fig. 1. A graphical representation of the relationship among fractional conversion, temperature and reaction rate for exothermic reaction [8].

2. 1-D integrated reaction and heat exchange model

A 1-D integrated reaction and heat exchange model for a parallel plate microreactor has been developed and is shown schematically in Fig. 2. The model repeats itself, therefore, requiring the boundaries ① and ② to be symmetric. Here, t is the wall thickness, and h, the half channel height. Since this is a simplified 1-D model, conduction along the wall (Section 2) is neglected. In addition, plug flow has been assumed for the heat exchange stream (Section 1), and ideal packed bed model has been adopted for the reactant stream (Section 3), which requires no transverse temperature gradient for both streams. The model also assumes no pressure drop, constant properties and no phase change.

From the control volume of the heat exchange stream, shown in Fig. 2, the energy balance becomes:

$$\lim_{\Delta x\to 0}\frac{\int_{\Delta A}\boldsymbol{q}\cdot\boldsymbol{s}_{\mathrm{n}}\mathrm{d}A}{\Delta V} = \lim_{\Delta x\to 0}\left[\frac{-qb\Delta x}{bh_1\Delta x}+\frac{(q_{x+\mathrm{d}x,1}-q_{x,1})bh_1}{bh_1\Delta x}\right] = \frac{q}{h_1}+\frac{\mathrm{d}q_{x,1}}{\mathrm{d}x} \quad (2)$$

where b is the channel width. Since heat transport by conduction is small compared to the convective transport term, the heat flux for the heat exchange stream can be simplified to:

$$q_{x,1} = -k_{\mathrm{f},1}\frac{\mathrm{d}T_1}{\mathrm{d}x}+(\rho C_{\mathrm{P}})_1 u_1 T_1 \approx (\rho C_{\mathrm{P}})_1 u_1 T_1. \quad (3)$$

The heat flux, q, crossing the wall can be described with an overall heat transfer coefficient and the temperature difference between the reactant and the heat exchange stream.

$$q = U(T_1 - T_3) \quad (4)$$

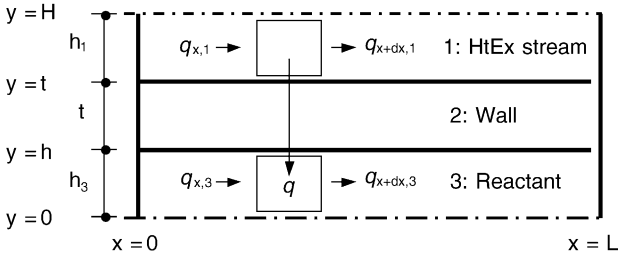

Fig. 2. Schematic diagram of the reactant and heat exchange model.

Combining Eqs. (2–4), the energy equation, Eq. (5), can be derived.

$$\frac{U(T_1 - T_3)}{h_1} + (\rho C_P)_1 u_1 \frac{dT_1}{dx} = 0 \quad (5)$$

The overall heat transfer coefficient, U, can be written in the form:

$$U = \frac{1}{1/h_{c,1} + t/k_w + 1/h_{c,3}} \quad (6)$$

where h_c is the surface-convective heat transfer coefficient, and k_w, the wall thermal conductivity. For the heat exchange stream, the surface-convective heat transfer coefficient is:

$$h_{c,1} = \frac{Nu_1 \times k_{f,1}}{D_h} = \frac{Nu_1 \times k_{f,1}}{4h_1} \quad (7)$$

where D_h is the hydraulic diameter. For the parallel plate geometry of the microreactor, in the case of uniform wall temperature and constant heat flux, the Nusselt numbers have been reported to be 7.54 and 8.23, respectively [9]. This study assumed a Nusselt number of 8.0. For the reactant stream, the surface-convective heat transfer coefficient is:

$$h_{c,3} = \frac{Nu_3 \times k_e}{D_h} = \frac{Nu_3 \times k_e}{4h_3}. \quad (8)$$

Classical analysis of the effective conductivity of packed beds provides that k_e can be written in terms of the porosity of the packed bed (ε), the conductivity of the reactant fluid and the catalyst.

$$k_e = \varepsilon \times k_{f,3} + (1 - \varepsilon) k_{cat} \quad (9)$$

The Nusselt number for packed bed of particles for ideally insulated plates can be written in the form [9]:

$$Nu_3 = 2 + (0.4 Re_{D_p}^{1/2} + 0.2 Re_{D_p}^{2/3}) Pr^{0.4} \quad (10)$$

where D_p and Re_{D_p} are defined as:

$$D_p = \frac{6V_s}{A_{ku}}, \quad Re_{D_p} = \frac{\rho_f u_f D_p}{\mu_f (1 - \varepsilon)}. \quad (11)$$

V_s is the volume of the solid portion, A_{ku}, the interfacial surface area and ε, the porosity of the packed bed. The porosity of the bed was assumed to be 0.40, which is a typical value for a randomly packed bed of monosized spherical particles.

For the reactant stream, plug flow is assumed, and the energy equation can be written in the form [10]:

$$\frac{dT_3}{dx} = A_C \times \frac{q''' + (-r)(-\Delta H_{Rx})}{\sum F_i C_{P,i}}. \quad (12)$$

For parallel plates, the energy balance equation (Eq. (12)) becomes:

$$\frac{dT_3}{dx} = bh_3 \times \frac{q \cdot 2bL/(2bh_3 L) + (-r)(-\Delta H_{Rx})}{\sum F_i C_{P,i}} = bh_3 \times \frac{q \cdot (1/h_3) + (-r)(-\Delta H_{Rx})}{\sum F_i C_{P,i}}. \quad (13)$$

Using the following relationship to describe the rate of change of the catalyst weight along the length:

$$dw = \rho_b A_C dx = \rho_b b h_3 dx. \quad (14)$$

Eqs. (5) and (13) can be rearranged to catalyst weight differential form

$$\frac{dT_1}{dw} = \frac{(U/\rho_b b h_3)(T_3 - T_1)}{(\rho C_P)_1 u_1 h_1} \quad (15)$$

$$\frac{dT_3}{dw} = \frac{(q/\rho_b h_3) + (-r')(-\Delta H_{Rx})}{\sum F_i C_{P,i}} \quad (16)$$

where r' is reaction rate per grams of catalyst. Eqs. (15) and (16) can be solved simultaneously with ideal plug flow mole-balance equations for each species.

$$\frac{dF_i}{dw} = r_i \quad (17)$$

The above formulations of the 1-D integrated reaction and heat exchange model were implemented using custom codes developed in POLYMATH 5.1, a commercial software package for numerical analysis.

3. 2-D integrated reaction and heat exchange model

The 1-D model developed in the previous section assumes that the longitudinal heat conduction through the wall is negligible, which is only valid for good insulating materials with very low thermal conductivity values. In order to extend to higher thermal conductivities, where the 1-D model is limited, a 2-D integrated reaction and heat exchange model has been developed and implemented using the finite element commercial software, FemLab. To avoid solving continuity and momentum equations for the heat exchange fluid, a parabolic velocity profile has been assumed. For the reactant stream, since the flow through the packed bed of catalyst pellets resembles the flow through a porous structure, the transverse velocity component has been assumed to be zero. The pressure drop along the length of the channel for the reactant stream has been investigated using the Ergun equation and was found to be less than 1% of the original inlet pressure. Pressure drops for both channels are therefore neglected.

For the heat exchange stream, only the heat transfer equation (Eq. 18) needs to be solved since parabolic velocity profile has been assumed.

$$\nabla.(-k_1 \nabla T_1 + (\rho C_P)_1 \boldsymbol{u_1} T_1) = 0 \quad (18)$$

The boundary conditions used are described below.

$$T_1 = T_{in} @ x = 0, \quad t \le y \le H \quad (19)$$

$$\frac{\partial T_1}{\partial y} = 0 \,@\, y = H, \quad \forall x. \quad (20)$$

Assuming the heat transport out of the system is dominated by convection, the exit boundary condition becomes

$$q_{x,1} = (\rho C_P T_1 u_1),\ -k_1 \frac{\partial T_1}{\partial x} = 0 \,@\, x = L, \quad t \le y \le H, \tag{21}$$

where $q_{x,1}$ is the heat flux.

For the wall, the conduction heat equation is used to model the 2-D heat transfer between the reactant and the heat exchange stream.

$$\nabla \cdot (-k_2 \nabla T_2) = 0 \tag{22}$$

Adiabatic boundary conditions are applied:

$$\frac{\partial T_2}{\partial x} = 0 \,@\, x = 0 \text{ and } x = L, \quad h \le y \le t \text{ (adiabatic)}. \tag{23}$$

For the reactant stream, conservation of species i is described by:

$$\nabla \cdot (-D_i \nabla C_i + C_i u_1) = r_i. \tag{24}$$

The total mass diffusivity coefficient for each specie, D_i, is defined as [11]:

$$D_i = D_{e,i} + D_i^d \tag{25}$$

where D_e is the effective mass diffusion coefficient, and D^d is the mass dispersion coefficient. Since the exact values of the effective mass diffusion coefficient and mass dispersion coefficient were not available, order of magnitude values from the literature [10] were used for the entire reactor bed. For gas–solid catalytic reactions taking place in packed bed reactors, D^d is estimated to be 4×10^{-5} by experimental findings, and the typical value of D_e for gas is 1×10^{-5} [10]. Thus, the effective total mass diffusivity is assumed to be 5×10^{-5} for all the species. The Peclet number, $Pe = uL/D_i$, was calculated to be much larger than 1 for current simulation conditions, thereby indicating the diffusion effects are minor or even negligible compared to convective effects. The boundary conditions used are described below.

$$C_i = C_{in} \,@\, x = 0, \quad 0 \le y \le h, \tag{26}$$

$$\frac{\partial C_i}{\partial y} = 0 \,@\, y = 0, \quad \forall x \text{ (symmetry)}, \tag{27}$$

$$\frac{\partial C_i}{\partial y} = 0 \,@\, y = h, \quad \forall x \text{ (insulation)}. \tag{28}$$

Assuming species transport is dominated by convection, the exit condition becomes

$$\bar{q}_{x,i} = C_i u_3, \quad -D_i \frac{\partial C_i}{\partial x} = 0 \,@\, x = L, \quad 0 \le y \le h, \tag{29}$$

where $\bar{q}_{x,i}$ is the molar flux.

From the theory of heat transfer in porous media [11], the energy equation for the reactant stream becomes

$$[\varepsilon(\rho C_P)_{f,3} + (1-\varepsilon)(\rho C_P)_{s,3}]\frac{\partial T}{\partial t} + (\rho C_P)_{f,3} \boldsymbol{u}_D \cdot \nabla T = (\rho C_P)_{f,3} \nabla (\boldsymbol{D} \cdot \nabla T) + Q, \tag{30}$$

where the total diffusivity tensor is defined as

$$\boldsymbol{D} = \frac{\boldsymbol{k}_e}{(\rho C_P)_{f,3}} + \varepsilon \boldsymbol{D}^d. \tag{31}$$

For the case of steady state, constant properties and dropping the dispersion term for the total diffusivity tensor yield:

$$-\nabla \cdot (k_e \cdot \nabla T) + (\rho C_P)_{f,3} u_D \cdot \nabla T = Q \tag{32}$$

where u_D is the Darcean velocity. Due to significant temperature variation in the longitudinal direction, the velocity will vary with respect to the reactor length. With the assumption of ideal gas law for the reactant, the volumetric flow rate is expressed as [10]:

$$v = v_0 \left(\frac{F_T}{F_{T,0}}\right)\left(\frac{P_0}{P}\right)\left(\frac{T}{T_0}\right) \tag{33}$$

For constant cross-sectional area with isobaric condition (no pressure drop) and noting that the number of moles of the product and the reactant is equal, i.e. $F_T = F_{T,0}$, the reactant stream velocity is expressed in the following form:

$$u_D = u_0 \left(\frac{T}{T_0}\right). \tag{34}$$

The volumetric heat generation term, Q, in Eq. (32) is defined as:

$$Q = (-r)(-\Delta H_{Rx}). \tag{35}$$

The effective conductivity has been defined previously in Eq. (9). The boundary conditions are taken as:

$$T_3 = T_{in} \,@\, x = 0, \quad 0 \le y \le h \tag{36}$$

$$\frac{\partial T_3}{\partial y} = 0 \,@\, y = 0, \quad \forall x \text{ (symmetry)} \tag{37}$$

and assuming convection dominated exit conditions:

$$q_{x,3} = (\rho C_P)_3 T_3 u_D, \quad -k_e \frac{\partial T_3}{\partial x} = 0 \,@\, x = L, \quad 0 \le y \le h. \tag{38}$$

4. Reaction rate equations and simulation conditions

The rate equation used in the simulation is adopted from Mizsey [12] and is presented below.

$$r' = k_3 P_{CO} P_{H_2O}\left(1 - \frac{P_{CO_2} P_{H_2}}{K_3 P_{CO} P_{H_2O}}\right) \quad (\text{mol/g} - \text{cat s}) \tag{39}$$

where $k_3 = 0.00225 \exp(-50{,}000/RT)$ in mol/g-cat s kPa^x and $K_3 = 9.543 \times 10^{-3} \exp(39{,}876/RT)$.

The catalyst used in Mizsey's study was 5 wt.% copper on alumina supplied by Johnson–Matthey plc, UK. Crushed catalyst particle size used in the experiment ranged from 0.25 mm to 0.5 mm. For the simulation, particle diameter and

Table 1
Model geometry and physical parameters

Parameter	Value
Channel width (b)	40 mm
Channel height ($2h$)	1 mm
Channel length (L)	40 mm
Wall thickness (t)	1 mm
Bulk catalyst density (ρ_b)	1×106 g/m^3
Inlet pressure	303 kPa
Catalyst conductivity (k_{cat})	0.4 W/m K
Reactant heat capacity ($C_{P,3}$)	1687.7 J/kg K
Reactant thermal conductivity (k_3)	0.1181 W/m K
Air density (ρ_1)	0.883 kg/m^3
Air heat capacity ($C_{P,1}$)	1009 J/kg K
Air thermal conductivity (k_1)	0.0331 W/m K
Water density (ρ_1)	975.7 kg/m^3
Water heat capacity ($C_{P,1}$)	4213 J/kg K
Water thermal conductivity (k_1)	0.665 W/m K

the bulk catalyst density are assumed to be 0.3 mm and 1×10^6 g/m^3, respectively.

Simulation geometries and physical parameters are summarized in Table 1. Constant properties are assumed for the heat exchange medium: air or water. For the reactant, volume-averaged values at 600 K are used for k_3 and $C_{P,3}$. For the heat exchange fluid, values for ρ_1, k_1 and $C_{P,1}$ are evaluated at 400 K for the air and 350 K for the water.

Since the reactant is assumed to follow the ideal gas law, the concentration change due to temperature variation results in variation of the reactant density.

$$\rho_3 = \text{mw} \times \sum_i C_i = \text{mw} \times \left(\frac{P}{RT}\right) \tag{40}$$

A typical exit stream composition of a steam reformer (SR) or autothermal reactor (ATR) consists of 25–75% H_2, 1–15% CO, 5–20% CO_2, 10–60% N_2 and a water-to-CO mole ratio between 2 and 15 [2]. The inlet conditions used in the simulations are summarized in Table 2.

5. Accuracy limit of the 1-D model and simulation approach

To investigate the accuracy limit of the 1-D model resulting from the assumption of negligible longitudinal wall conduction, comparative studies using both the 1-D and 2-D models were undertaken. The results from the comparative study of the parallel flow arrangement are shown in Figs. 3 and 4. As the thermal conductivity of the wall increases, the 1-D temperature profiles deviate from the 2-D results. A similar trend in the results was also observed for the counter flow microreactor arrangement. This behavior is expected due to the assumption that the longitudinal conduction of the wall is neglected in the 1-D model. The assumption is valid only for heat transfer through very thin walls, and as the wall thickness increases, the effect of longitudinal conduction becomes significant. For the current simulation geometries, the wall thickness and the channel height is of the same order of magnitude, and thus 1-D model is valid only for low wall thermal conductivities.

For the parametric study, results obtained from the 2-D model are used for simulation conditions involving high wall thermal conductivities, and the 1-D model results are used for low wall thermal conductivity simulation cases in order to gain computational efficiency.

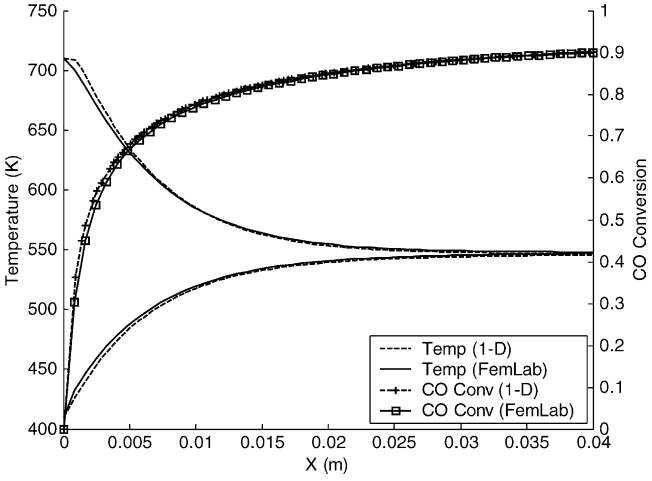

Fig. 3. Parallel flow WGS reactor temperature profile (k_w = 0.03 W/m K).

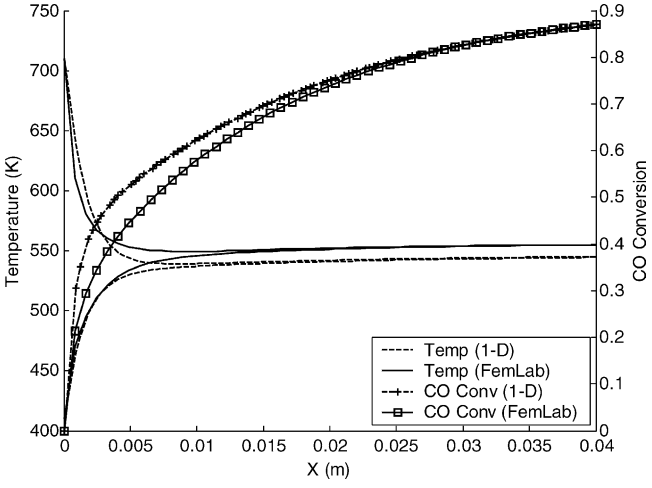

Fig. 4. Parallel flow WGS reactor temperature profile (k_w = 1.0 W/m K).

Table 2
Reactant gas composition and feed

	CO	H_2O	CO_2	H_2	N_2
Gas composition (%)	6	25	10	29	30
Molar flow rate (mol/s)	1.56×10^{-5}	6.5×10^{-5}	2.6×10^{-5}	7.54×10^{-5}	7.8×10^{-5}

6. Parametric study of integrated micro-WGS reactor

6.1. Effect of temperature profile on CO conversion

To investigate the effect of temperature profile on the CO conversion, various possible temperature profiles were modeled using polynomial functions and applied in the 1-D model to determine resultant CO conversion. Five different temperature profiles were considered with identical inlet and exit temperatures. The five profiles and their corresponding calculated CO conversion levels are presented in Fig. 5. As the temperature profiles change from concave to convex profiles, the maximum CO conversion is observed, again evidencing the existence of an optimal temperature profile. The highest conversion is achieved when the temperature profile is convex, which means quick extraction of heat is required at the entrance. With high inlet temperature, the reaction rate is fast, reaching equilibrium conversion very quickly, and therefore the reactant temperature must be lowered quickly in order to yield high CO conversion. The convex temperature profile resembles that of either a counter or a parallel flow heat exchanger temperature profile, which supports the proposal that the integration of reactor and heat exchanger may result in better performance. It is also worthwhile to note that after reaching maximum CO conversion, a faster drop in the reactant temperature does not lower the CO conversion significantly.

6.2. Parametric study of integrated micro-WGS reactor performance

A parameter set was selected accordingly to yield 90% CO conversion with a highest reactant flow rate possible. This set was considered as the optimal parameter set for the given reactant flow rate. Then, each parameter has been varied to investigate the effect on CO conversion with other parameters set to the optimum values. Parameters selected for the investigation are the wall thermal conductivity, the inlet temperature and velocity of the heat exchange stream, and the inlet temperature and velocity of the reactant stream. For each parameter, two types of flow configurations have been investigated: parallel flow (P) and counter flow (C). A set of parameter ranges, for a minimum CO conversion of 85%, is summarized in Table 3.

Table 3
Summary of parameter ranges for 85% CO Conversion (heat exchange medium: air)

Parameter	Parallel	Counter
Thermal conductivity (W/m K)	0.006 ∼ 0.3	0.015 ∼ 200
Heat exchange fluid temperature (K)	298 ∼ 496	472 ∼ 592
Heat exchange fluid velocity (m/s)	0.39 ∼ 4.8	0.43 ∼ 12
Reactant temperature (K)	621 ∼ 710	540 ∼ 710
Reactant velocity (m/s)	0.245 ∼ 0.41	0.245 ∼ 0.41

The effect of wall thermal conductivity on CO conversion for both the parallel flow and counter flow configurations can be clearly observed in Fig. 6. As the thermal conductivity increases, CO conversion reaches a maximum value (90.0%) and decreases asymptotically to a final value. At very high thermal conductivity, thermal washout occurs and the two temperatures quickly converge, and no further variation of temperature profile can be obtained by increasing the wall conductivity.

To achieve CO conversion higher than 85%, the parallel flow scheme requires the wall conductivity to be very low, in the range of 0.006–0.3 W/m K. It is very difficult to achieve such insulating conditions with commonly used engineering materials. However, for the counter flow arrangement, a higher CO conversion is obtained for a much wider range of wall thermal conductivity as shown by the plateau of the CO conversion level extending through the full simulation range up to a maximum thermal conductivity of

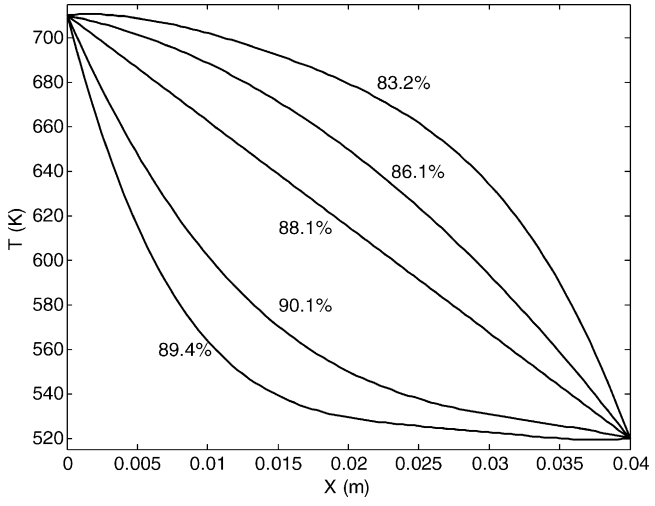

Fig. 5. CO conversion with different temperature profiles.

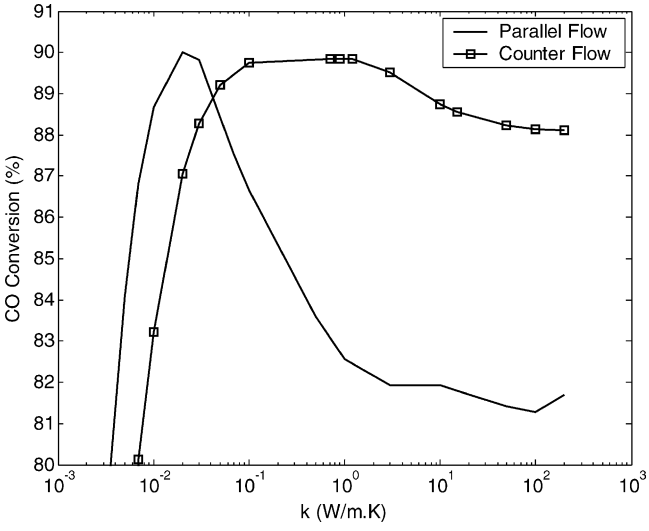

Fig. 6. Thermal conductivity vs. CO conversion for both parallel and counter flow (air).

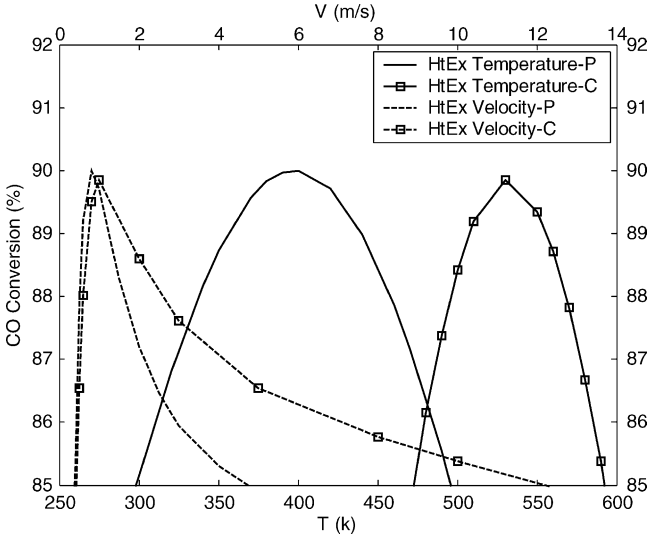

Fig. 7. Effects of inlet temperature and velocity of the heat exchange stream on CO conversion for both parallel and counter flow configurations (air).

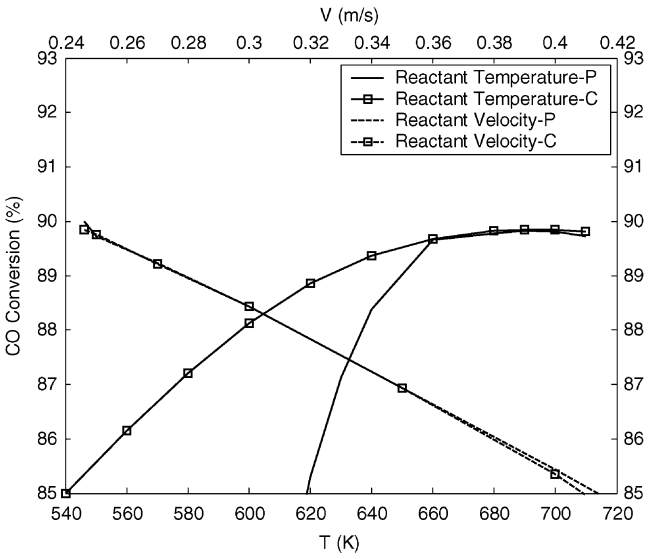

Fig. 8. Effects of inlet temperature and velocity of the reactant stream on CO conversion for both parallel and counter flow configurations (air).

200 W/m K. A material having thermal conductivity higher than 0.015 W/m K can achieve 85% CO conversion. The significance of this result should be interpreted in terms of the marked simplification of the manufacturing challenges inherent in microreactor fabrication that is achieved through broader range in material selection. Reactors typically used for high temperature applications are made of stainless steel or inconel, which have thermal conductivity in the range of 10–17 W/m K. The study confirms that these engineering materials may still be used for integrated reactors without degradation of performance.

The effect of inlet temperature and velocity of the heat exchange stream on reactor performance is shown in Fig. 7. The temperature range to achieve CO conversion higher than 85% is wider and lower for the parallel flow configuration. Lower heat exchange temperature requires less energy for heating, improves overall system thermodynamic efficiency and makes it easy to capture heat from other exothermic reactions in the system. The effect of inlet velocity of heat exchange stream can be observed in Fig. 7. The highest conversion for both parallel and counter flow configuration is obtained at similar velocities, however, the velocity range over which 85% conversion can be achieved is much wider for counter flow scheme. Thus, for parallel flow, more sensitive control of the velocity is required to maintain necessary performance.

The effect of the reactant flow rate on the CO conversion is similar for parallel and counter flow schemes, showing quasi-linear behavior (refer to Fig. 8). However, for the reactant temperatures, counter flow has a wider permissible range for 85% conversion than parallel flow. For the counter flow reactant temperatures may be lowered to 540 K and still achieve CO conversion of 85%, while for the parallel flow reactant temperatures should be higher than 621 K. The sensitivity of the microreactor performance in terms of the reactant inlet temperature is an important consideration. Designs that are less sensitive to inlet temperature variations are favorable since they are better able to tolerate the inherent variations in the output of the upstream components of the complete fuel processing system. The low sensitivity of the inlet reactant temperature to CO conversion curve for the counter flow arrangement is therefore more desirable in integrated micro-WGS reactor design.

6.3. *Effect of heat exchange medium on micro-WGS reactor performance*

The integrated reaction model has also been used to study the performance of the reactor using liquid water as the heat exchange medium. The results are shown in Figs. 9 and 10.

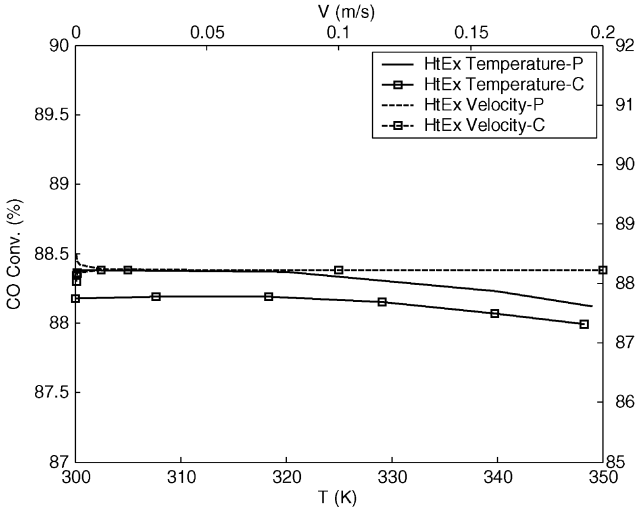

Fig. 9. Effects of inlet temperature and velocity of the heat exchange stream on CO conversion for both parallel and counter flow configurations (water).

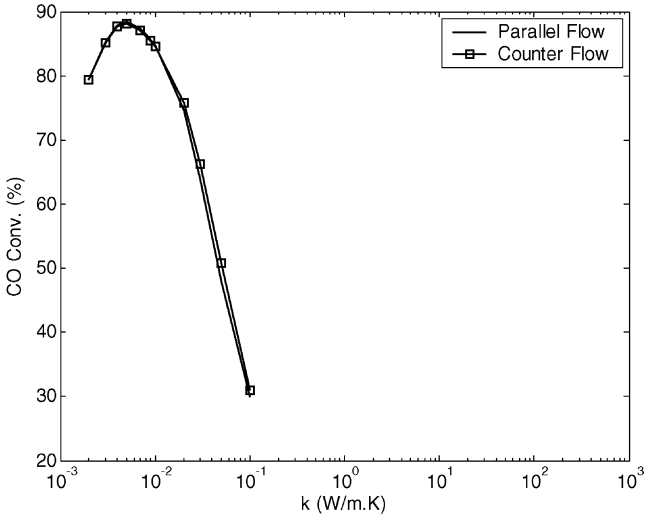

Fig. 10. Thermal conductivity vs. CO conversion for both parallel and counter flow configurations (water).

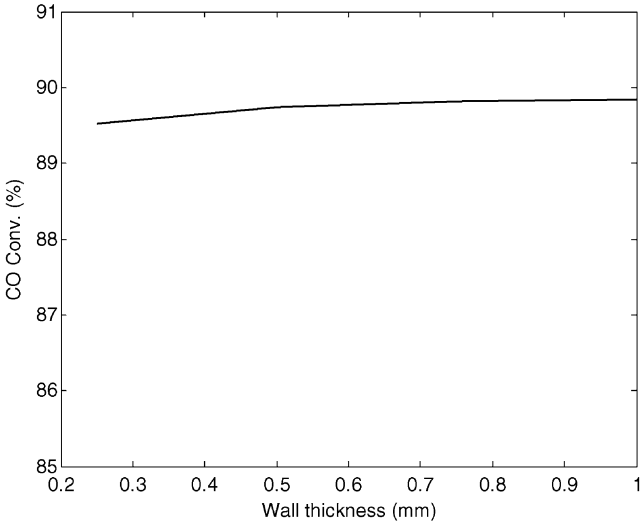

Fig. 11. Effect of wall thickness on the CO conversion.

For both parallel and counter flow, the heat exchange fluid temperature and velocity have little effect on the CO conversion. Phase change occurs for high inlet temperature and low feed velocity.

The results of the simulation of the liquid water heat exchange medium also indicates that the thermal conductivity needed to maintain high conversion is very small, around 0.005 W/m K, for both counter and parallel flow arrangement. Such an insulating condition is very difficult to meet. In addition, CO conversion drops sharply as the wall thermal conductivity increases.

7. Performance advantages and miniaturization potential of the integrated micro-WGS reactor designs

A comparison between integrated and adiabatic reactor performance has been undertaken in terms of the catalyst amount used. Adiabatic simulations were performed by forcing the heat flux term, q in Eq. (16), to zero. For both reactors, parameters are selected so as to achieve reactor performance of 90% CO conversion with highest inlet feed flow rate possible. The catalyst weight and volume has been scaled to give 0.011 mol/s of hydrogen, which is the estimated amount required to drive 1 kW fuel cell. The results of the comparative study are presented in Table 4. The results show that 90% CO conversion can be achieved with half the catalyst amount with the integrated design.

Table 4
Comparison between adiabatic and integrated reactor

Reactor	Catalyst weight (g)
Adiabatic	206.4
Integrated (t = 1 mm)	98.8

To investigate the miniaturization potential of the integrated design for WGS process, effect of wall thickness on CO conversion has been studied. Fig. 11 shows the CO conversion for different wall thickness with all other conditions being the same. The result indicates the thickness of the reactor wall does not have much influence on the CO conversion. The wall thickness should be fabricated as thin as possible for further reducing the size of the reactor, and therefore improving the power density of the entire fuel cell system. For 1 kW system, the integrated design requires 62 reactant channels, and the total reactor volume required is 246.6 ml assuming the wall thickness to be 0.25 mm. For the adiabatic reactor, 129 channels are required, and the reactor volume is 206.4 ml. Since the adiabatic reactor requires external heat exchanger to provide corresponding inlet reactant temperature, fair comparison regarding the reactor volume cannot be made between the adiabatic and the integrated design. If the total fuel processing system is considered, integrated heat exchanger design offers potential for size reduction.

8. Conclusions

This study has introduced and developed an integrated heat exchange and reaction design for microreactors. The integrated design enables the integration among various components in a system through a heat exchange medium. The model has been utilized to perform a parametric study on WGS reaction to characterize the integrated microreactor performance.

The study investigated sensitivity of the reactor performance to changes in selected design parameters (wall thermal conductivity, heat exchange medium, inlet temperature and velocity) for two types of flow arrangement, counter and

parallel flow, and suggested general operating ranges for these parameters to achieve CO conversion of at least 85%. For both parallel and counter flow reactor, there existed an optimal range of wall thermal conductivity. However, the range of acceptable thermal conductivities for the parallel flow configuration was narrow and limited to application of insulating materials. Thus, when considering mass production of the microreactors, the counter flow arrangement is favorable since the resultant extension of the range of optimal thermal conductivities enables the selection of traditional engineering materials, thereby lowering material costs and improving producibility. The integrated microreactor design showed significantly different behavior with liquid water as the heat exchange medium. For both parallel and counter flow, heat exchange stream temperature and velocity had little effect on the CO conversion. Required wall thermal conductivity was also very small, around 0.005 W/m K, to achieve CO conversion level of 90%. Comparison between adiabatic and integrated reactor showed that the integrated reactor needed only the half the catalyst weight, which indicates more efficient use of the catalyst.

Acknowledgements

The financial support from the Department of Energy and technical assistance from the Chemical Engineering Department at the University of Michigan are gratefully acknowledged.

References

[1] A.Y. Tonkovich, J.L. Zilka, M.J. LaMont, Y. Wang, R.S. Wegeng, Microchannel reactors for fuel processing applications. 1. Water gas shift reactor, Chem. Eng. Sci. 54 (1999) 2947–2951.
[2] R.L. Keiski, T. Salmi, V.J. Pohjola, Development and verification of a simulation model for a non-isothermal water-gas shift reactor, Chem. Eng. J. 48 (1992) 17–29.
[3] A. Beenackers, G.P.v.d. Laan, Intrinsic kinetics of the gas-solid fischer-tropsch and water gas shift reactions over a precipitated iron catalyst, Appl. Catal. A: General 193 (2000) 39–53.
[4] D. Andreeva, V. Idakiev, T. Tabakova, L. Ilieva, P. Falaras, A. Bourlinos, A. Travlos, Low temperature water gas shift reaction over Au/CeO2 catalysts, Catal. Today 72 (2002) 51–57.
[5] M. Levent, Water gas shift reaction over porous catalyst: temperature and reactant concentration distribution, Int. J. Hydrogen Energy 26 (2001) 551–558.
[6] T. Salmi, L. Lindfors, S. Bostrom, Modeling of the high temperature water gas shift reaction with stationary and transient experiments, Chem. Eng. Sci. 41 (1986) 929–936.
[7] P. Harriott, Chemical Reactor Design, Marcel Dekker, Inc., New York, 2003.
[8] R.E. Hayes, Introduction to Chemical Reactor Analysis, Golden and Breach Science Publishers, 2001.
[9] M. Kaviany, Principles of Heat Transfer, John Wiley & Sons, Inc., New York, 2002.
[10] H.S. Fogler, Elements of Chemical Reaction Engineering, 3rd ed., Prentice-Hall International, 1999.
[11] M. Kaviany, Principles of Heat Transfer in Porous Media, 2nd ed. New York, 1999.
[12] P. Mizsey, E. Newson, T.-b. Truong, P. Hottinger, The kinetics of methanol decomposition: a part of autothermal partial oxidation to produce hydrogen for fuel cells, Appl. Catal. A: General 213 (2001) 233–237.